Assembly of viral capsids, buckling, and the Asaro-Grinfeld-Tiller instability

Alexander Yu. Morozov and Robijn F. Bruinsma
Department of Physics and Astronomy, University of California–Los Angeles, Los Angeles, California 90024, USA
(Received 28 December 2009; published 30 April 2010)

Icosahedral viral shells are characterized by *intrinsic elastic stress* focused on the 12 structurally required pentamers. We show that, according to thin-shell theory, *assembling* icosahedral viral shells should be subject to the *Asaro-Grinfeld-Tiller instability* (AGTI). AGTIs are encountered in growing epitaxial films exposed to extrinsic elastic stress. For viral shells, the AGTI relieves intrinsic elastic stresses by generating corrugation along the perimeter of the assembling shell. The *buckling transition* of Lidmar, Mirny, and Nelson provides an alternative mechanism for stress release, which in principle would allow for avoidance of AGTIs. For system parameters appropriate for viral shells however, the AGTI appears to be unavoidable. The azimuthal stress condensation produced by the AGTI might actually assist assembly by providing a guiding mechanism for the insertion of pentamers during viral assembly.

DOI: 10.1103/PhysRevE.81.041925 PACS number(s): 87.16.dr, 87.15.nr, 87.15.km, 87.10.Pq

I. INTRODUCTION

The genome molecules of viruses are enclosed by a shell of proteins: the "capsid." High-resolution crystallography studies [1] reveal that the capsid proteins ("subunits") are assembled into a precisely ordered structure, which otherwise is unusual for protein aggregates. Spherical capsids usually have icosahedral symmetry, with the subunits grouped in protein pentamers and hexamers ("capsomers") [2]. Notwithstanding the considerable structural complexity of these icosahedral capsids, viral shells often assemble spontaneously from supersaturated solutions of subunits provided thermodynamic parameters such as acidity and salinity are set appropriately [3]. Subunits interact through a combination of electrostatic repulsion and hydrophobic attraction. Varying the acidity and salinity conditions adjusts the relative balance between these competing interactions, thereby favoring assembly or disassembly [4]. Thermodynamic studies of viral self-assembly report that the strength of these subunit-subunit interactions typically is in the range of $(5-10)k_BT$ [5]. Although the structure of many fully assembled shells is known in great detail, it has proven remarkably difficult to reconstruct *how* a viral shell is assembled. It is believed that viral shells grow on a "capsomer-by-capsomer" basis, much like crystals, by continued addition of subunits. Individual subunits or small oligomers diffuse in from the aqueous solution to partially assembled shells and are added along the growth perimeter. These initial interactions appear to be relatively weak [6], with high "off rates."

In this paper we will borrow concepts from the theory of the growth of conventional crystals and apply them to the assembly of viral shells. A viral shell can be viewed as a curved two-dimensional crystal with *intrinsic elastic strain*. Caspar and Klug, two pioneers of viral crystallography, used basic symmetry arguments to show that the internal structure of the subunits necessarily is *deformed* with respect to a perfect hexagonal sheet [2]. They introduced the "model" icosahedral viral shell composed of 12 pentamers and $10(T-1)$ hexamers, with T as an integer, arguing that this construction minimizes subunit deformations ("quasiequivalence"). By quantitatively applying the principle of minimum elastic energy to thin elastic shells with icosahedral symmetry, Lidmar *et al.* [7] showed that for smaller shells the *bending energy* dominates, which leads to shells with a spherical shape while for larger shells, the *stretching energy* dominates. In the latter case, the 12 fivefold symmetry sites buckle out: the "buckling transition." A transition from predominantly spherical to predominantly polyhedral shape for increasing shell size indeed can be observed *grosso modo* in a catalog of capsid structures.

It is well known that elastic stresses have drastic effects on the growth of conventional crystals: they produce *growth defects* [8]. If a crystal is grown from a (supersaturated) vapor on a substrate with a different lattice constant ("heteroepitaxy") then the first few layers of the growing crystal often adopt the lattice constants and symmetry structure of the substrate, with the result that they are elastically strained. The elastic energy of these "commensurate" overlayers is proportional to the film thickness. Eventually, this growing elastic energy is released either by the nucleation of topological defects ("misfit dislocations") or by the nucleation of microcrystallites with the equilibrium lattice constant. Linear stability analysis of a semi-infinite elastic material under a uniaxial, externally applied stress reveals that, as the layer thickness grows, an unstable mode develops with a characteristic wavelength determined by the ratio of the surface energy and the bulk elastic modulus of the crystal [9]. This "Asaro-Grinfeld-Tiller instability" (AGTI) is *not* related to Euler buckling—it takes place both for stretching and compression—and it is believed to be the main precursor of the formation of microcrystallites. The aim of this paper is to examine the implications of the minimum elastic energy condition for *incomplete shells*—as opposed to fully assembled shells—and to check if AGTI-type instability interferes with viral shell assembly. We will do this by applying the continuum theory of thin elastic shells developed by Nelson and Seung (NS) [10]. Our first step is to extend the NS method to include the "capillary" stresses generated by the perimeter of the incomplete shell and the "curvature" stress generated by the spontaneous curvature of a sheet of capsid proteins.

II. CONTINUUM ELASTICITY THEORY OF INCOMPLETE SHELLS WITH PREFERRED CURVATURE

In thin-shell continuum theory, the elastic energy F_e of a thin layer of material is written as the sum of a bending energy, a stretching energy, and a dilation energy. The bending energy is given by

$$F_b = \frac{\kappa}{2}\int d^2s(H-2/R)^2 - \bar{\kappa}\int K d^2s. \tag{1}$$

Here, H is the local mean curvature of the shell, while $2/R$ is the spontaneous or preferred curvature of the shell. Next, K is the local Gauss curvature while κ and $\bar{\kappa}$ are moduli with dimension of energy. We will assume both moduli to be positive. Spontaneous curvature is assumed to be the determinant of the size of the fully assembled shell with the "spontaneous curvature" radius R identified as the radius of the fully assembled shell. A closed spherical shell of radius R minimizes F_b for positive κ and $\bar{\kappa}$. The sum of stretching and dilation energies can be expressed as

$$F_s = \tfrac{1}{2}\int d^2s\sigma_{\alpha\beta}u_{\alpha\beta}, \tag{2}$$

with $\sigma_{\alpha\beta}$ as the two-dimensional (2D) stress tensor and $u_{\alpha\beta}$ as the strain tensor. For a small, partially formed shell, the strain tensor can be expressed in terms of the in-plane displacement $\vec{u}(\vec{r})$ of the shell, with $\vec{r}$ as a Cartesian coordinate in the reference plane shown in Fig. 1, and of the out-of-plane displacement $\zeta(\vec{r})$ of the shell with respect to a reference plane in the Monge representation (see Fig. 1):

$$u_{\alpha\beta} = \frac{1}{2}\left(\frac{\partial u_\alpha}{\partial x_\beta} + \frac{\partial u_\beta}{\partial x_\alpha}\right) + \frac{1}{2}\frac{\partial\zeta}{\partial x_\alpha}\frac{\partial\zeta}{\partial x_\beta}. \tag{3}$$

If, for example, a constant mean curvature H is imposed on a flat circular sheet then this introduces a strain of the order of $H^2\rho^2$, with ρ as the distance to the origin. In terms of the out-of-plane displacement, the Gauss curvature equals $K(\vec{r}) = \zeta_{xx}\zeta_{yy} - \zeta_{xy}^2$. For a sheet with hexagonal symmetry, apart from isolated defects, the relation between stress and strain tensors is given by

$$u_{\alpha\beta} = Y^{-1}[(1+\nu)\sigma_{\alpha\beta} - \nu\delta_{\alpha\beta}\sigma_{kk}], \tag{4}$$

with Y as the (2D) Young's Modulus and ν as the Poisson's ratio. For a completed shell of radius R, the ratio of stretching and bending energies is determined by the dimensionless "Foppl von Karman (FvK) number" YR^2/κ, introduced by Lidmar *et al.* [7]. For YR^2/κ large compared to 10^2, the shape of a (completed) shell is that of a facetted icosahedron while for YR^2/κ small compared to 10^2, it has a spherical shape.

Within the Gibbs theory of thermodynamics, the total assembly free energy of a patch of partial shell under elastic strain can be written as $\Delta G = F_e - \Pi A + \tau P$, with A as the shell area and P as the length of the perimeter of the incomplete shell. For the case of incomplete viral shells, the parameter Π can be identified with the *assembly free energy gain* per unit area of shell due to (favorable) subunit-subunit contacts but excluding the elastic energy costs given by F_e, which is neither proportional to A nor to P, as discussed below. The parameter τ can be identified with the *line energy cost* of the perimeter of the partial shell, representing the fact that subunits lining the perimeter of an incomplete shell will have more exposed hydrophobic residues and fewer favorable subunit-subunit contacts than subunits in the interior.

The minimization of the elastic energy for given A and P is simplified by introducing the Airy stress function χ with $\sigma_{xx} = \partial^2\chi/\partial y^2$, $\sigma_{yy} = \partial^2\chi/\partial x^2$, and $\sigma_{xy} = -\partial^2\chi/\partial x\partial y$. NS showed that minimization of the elastic energy with respect to the in-plane displacement leads to an inhomogeneous biharmonic equation for the stress function:

$$\Delta^2\chi(\vec{r}) + Y[K(\vec{r}) - s(\vec{r})] = 0. \tag{5}$$

Here, $K(\vec{r})$ is the local Gauss curvature and $s(\vec{r})$ is the local *disclination area density*. For viral shells mainly composed of hexagonal protein sheets, these disclinations are identified with the pentamers. We will examine two cases, namely shell growth "seeded" by a hexamer and growth seeded by a pentamer. In the first case, the partial shell initially has no pentamers while in the second case a single fivefold disclination is located at the origin, i.e., $s(\vec{r}) = (2\pi/6)\delta(\vec{r})$.

Equation (5) must be solved with the boundary condition that along the perimeter, the stress must compensate the capillary pressure exerted by the line energy, which leads to the condition that $\sigma_{ij}n_j = -\tau C n_i$, with $\hat{n}$ as the outward normal to the perimeter and with C as the local curvature of the perimeter. Once the Airy function has been found, the stretching or dilation contribution to the elastic energy can be expressed as

$$F_s = \frac{1}{2Y}\int d^2r\left\{(\Delta\chi)^2 - 2(1+\nu)\left[\frac{\partial^2\chi}{\partial x^2}\frac{\partial^2\chi}{\partial y^2} - \left(\frac{\partial^2\chi}{\partial x\,\partial x}\right)^2\right]\right\}. \tag{6}$$

The simplest shape for an incomplete shell would be a circularly symmetric *spherical cap* [11] with constant mean curvature. The projection on the reference plane tangent to center of the cap is then a circle with radius ρ_0. We will define an effective FvK number $\gamma = Y\rho_0^2/\kappa$ for incomplete shells and obtain the elastic energy for the different regimes of γ.

A. $\gamma \ll 1$

For γ small compared to one, the bending energy dominates the elastic energy. When the bending energy dominates, a mean curvature H close to $2/R$ is imposed on the cap [see Eq. (1)]. The out-of-plane displacement of the cap is then given by $\zeta(\vec{r}) \approx (1/2)r^2/R$ so the contribution to the strain tensor that depends on the out-of-plane displacement is $(1/2)x_\alpha x_\beta/R^2$. The Airy function that obeys the boundary conditions $\sigma_{ij}n_j = -(\tau/\rho_0)n_i$ for a spherical cap with a circularly symmetric border is easily found:

$$\chi(r) = \frac{Y}{64R^2}(2\rho_0^2 r^2 - r^4) + \left(\frac{sY}{8\pi}\right)r^2(\ln r/\rho_0 - 1/2) - \frac{\tau}{2\rho_0}r^2. \tag{7}$$

Here, $s=0$ for a shell composed of hexamers and

$s=2\pi/6$ if a pentamer is located at the origin. The stress tensor derived from $\chi(r)$ is written as $-(\tau/\rho_0)\delta_{ij}+\sigma_{ij}^0$. The first term is the *Laplace pressure* generated by the line energy. The remaining term is diagonal, with $\sigma_{rr}^0(r)=(Y/16R^2)(\rho_0^2-r^2)+(sY/4\pi)\ln r/\rho_0$ and $\sigma_{\theta\theta}^0(r)=(Y/16R^2)(\rho_0^2-3r^2)+(sY/4\pi)(\ln r/\rho_0+1)$ independent of the line energy. In both cases, the first term is the stress field introduced by the curvature imposed on the shell while the second term is the stress field of a disclination in a flat sheet characterized by logarithmic singularity at the origin. The total elastic energy of a circularly symmetric cap with $\gamma \ll 1$ is then

$$F_e \sim \begin{cases} \pi Y\rho_0^2\left[2\left(\frac{s}{8\pi}\right)^2-\frac{1}{8}\left(\frac{s}{8\pi}\right)\frac{\rho_0^2}{R^2}+\frac{1}{384}\frac{\rho_0^4}{R^4}\right]-\pi\rho_0^2\bar{\kappa}/R^2 & \Gamma \ll 1 \\ \frac{\pi(1-\nu)}{Y}\tau^2-\pi\rho_0^2\bar{\kappa}/R^2 & \Gamma \gg 1, \end{cases} \tag{8}$$

with $\Gamma=\tau/Y\rho_0$ as the dimensionless line energy. According to Eq. (8), the Gauss curvature term can be absorbed into a redefinition of Π. The elastic energy is however proportional to neither the area A nor to the perimeter P. Below, we will assume that ρ_0/R is small compared to one. According to Eq. (8), it is not energetically favorable for shells with ρ_0/R less than $\sqrt{2s/\pi}\sim 0.81$ to introduce a pentamer at the origin. However, viral assembly typically is an example of "heterogeneous nucleation", and the initial conditions could favor assembly starting from pentamers. Separately, assembly is often initiated by interaction between capsid proteins and genome molecules and in some cases this is known to favor assembly starting from pentamers [12,13].

B. $\gamma \gg 1$: No central pentamer

If there is no central pentamer, then the optimal shape of a circularly symmetric shell approximately remains that of a spherical cap even if $\gamma \gg 1$ but the mean curvature H will be less than $2/R$. The optimal value of H can be estimated by comparing the bending energy $F_b \sim \kappa\rho_0^2(H-2/R)^2$ of the cap with the stretching energy $F_s \sim Y\rho_0^2(H^2\rho_0^2)^2$ that is associated with a strain tensor $u_{\alpha\beta} \propto (H\rho_0)^2$. Minimizing F_s+F_b with respect to H then gives $(2/R)-H \propto (\gamma/\rho_0)(H\rho_0)^3$. Accordingly, smaller caps with $\gamma\rho_0^2/R^2 \ll 1$ still have a mean curvature H close to $2/R$ and the results of the previous section are not changed. For larger caps, with $\gamma\rho_0^2/R^2 \gg 1$, the mean curvature of the shell $H \sim R^{-1}/(\gamma\rho_0^2/R^2)^{1/3}$ decreases with increasing shell size. Note that this suggests that for a spherical cap with preferred curvature $Y\rho_0^4/\kappa R^2$ is a more appropriate measure for the ratio of bending and stretching energies than γ. The total elastic energy can then be estimated as $F_s/\kappa \sim (\kappa/Y\rho_0^2)^{1/3}(\rho_0^2/R^2)^{2/3}$ in this regime.

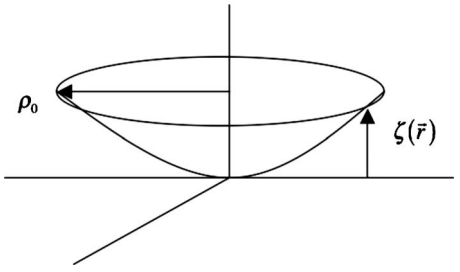

FIG. 1. Monge coordinate representation for a rotationally symmetric partial shell having a circular boundary of radius ρ_0. $\zeta(\bar{r})$ is the vertical displacement measured from a reference plane tangent to the partial shell at the center.

C. $\gamma \gg 1$: Central pentamer

The case of a circularly symmetric partial shell with a central pentamer is more challenging. The shell is expected to buckle based on the results of NS and resemble a cone with a flattened-out apex. The flattened section has a size of the order of the *buckling radius* $R_b=\sqrt{\kappa/Y}$. Inside the flattened section, the stretching energy "wins," while in the conical section the bending energy wins. We need to extend the results of NS to the case of shells with a preferred curvature radius. This is done most easily by introducing the following one-parameter trial form for the vertical displacement:

$$\zeta(r) = \sqrt{\frac{1}{3}}(r^2+b^2)^{1/2}. \tag{9}$$

For $r \gg b$, this trial form resembles a cone having an apex angle appropriate for a single $s=2\pi/6$ disclination at the origin. For $r \ll b$ it reduces to a spherical cap with curvature $\sqrt{s/\pi}(1/b)$ (from hereon, we will use $s=2\pi/6$). It is possible to obtain explicitly the Airy function and the stress distribution for this trial function, as discussed in the Appendix. The noncapillary contribution to the tangential elastic stress along the perimeter—the quantity of interest for thermodynamic stability of the perimeter—is for this trial function

$$\sigma_{\theta\theta}^0(r=\rho_0) = \frac{Y}{12}\left[\frac{b(\rho_0)}{\rho_0}\right]^2 \ln\left\{1+\left[\frac{\rho_0}{b(\rho_0)}\right]^2\right\}. \tag{10}$$

The variation parameter $b(\rho_0)$ is, in general, *not* equal to the buckling radius, as might have been expected intuitively. Figure 2 shows the dependence of $b(\rho_0)$ on the shell size (all lengths are expressed in units of the spontaneous curvature

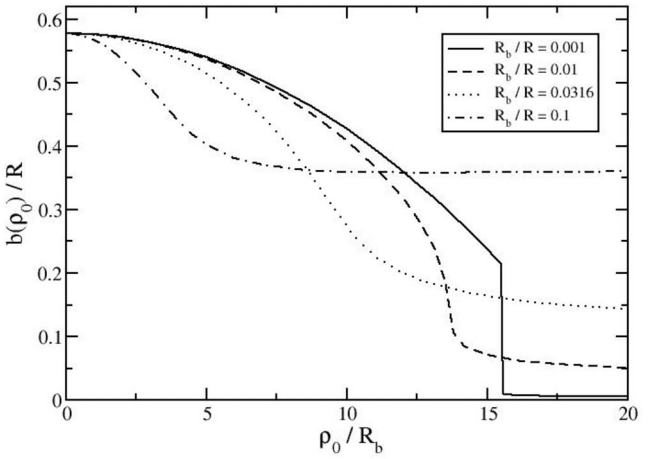

FIG. 2. Dependence of the variation parameter $b(\rho_0)$ in the variational shell shape $\zeta(r)=\sqrt{1/3}(r^2+b^2)^{1/2}$ on the shell radius ρ_0 for different values of the buckling radius R_b. Both $b(\rho_0)$ and R_b are expressed in units of the radius R of the fully assembled shell.

radius R) computed by numerical minimization of the elastic energy. If the buckling radius is small compared to the radius of spontaneous curvature R, then there is a sharp drop of $b(\rho_0)$ at a threshold ρ_b. We will identify this sharp drop with the buckling transition. In the Appendix we show that if $\rho_0 \ll b(\rho_0)$, then $b(\rho_0)$ is given by

$$b(\rho_0) \approx \sqrt{\frac{1}{3}}R\left(1-\frac{1}{384}(\rho_0^2/R_b^2)\right). \tag{11}$$

The shape of the trial shell is still that of a spherical cap but with a curvature $\sqrt{1/3}(1/b(\rho_0))$ that now exceeds $1/R$. According to Eq. (11), the shell curvature diverges when the disk radius approaches a size $\sqrt{384}R_b$, which thus is the buckling threshold ρ_b for the case that R is large compared to R_b. The requirement $\rho_0 \ll b(\rho_0)$ is valid if two conditions are satisfied: (i) $\rho_0 \ll R$ and (ii) ρ_0 must be less than $(\sqrt{384})R_b$. The noncapillary perimeter stress in this regime is given by

$$\sigma^0_{\theta\theta}(\rho_0) \sim \frac{Y}{36}\left(\frac{R}{\rho_0}\right)^2\left[1-\frac{1}{384}(\rho_0^2/R_b^2)\right]^2 \times \ln\left\{1+\frac{3\rho_0^2/R^2}{\left[1-\frac{1}{384}(\rho_0^2/R_b^2)\right]^2}\right\}. \tag{12}$$

According to Eq. (12), $\sigma^0_{\theta\theta}(\rho_0) \sim Y/12$ for small ρ_0. For increasing shell radius, the tangential stress starts to drop rapidly as ρ_0 approaches the buckling threshold.

In the opposite regime $\rho_0 \gg b(\rho_0)$, $b(\rho_0)$ is determined by the buckling radius as might be expected intuitively. In the Appendix, it is shown that $b(\rho_0) \approx (12/\pi)R_b[1+O(R_b^2/\rho_0^2)]$ for $\rho_0 \gg b(\rho_0)$. The shell shape reduces in this regime to a conical cap. The tangential stress along the perimeter decays in this regime as $\sigma_{\theta\theta}(\rho_0) \approx 24Y(R_b/\pi\rho_0)^2\ln(\pi\rho_0/12R_b)$, so roughly as the inverse square of the size of the conical cap. The validity conditions are $\rho_0 \gg (12/\pi)R_b$, but ρ_0 must be still less than R. Figure 3 shows the evolution of the cap shape with increasing ρ_0 across the buckling transition.

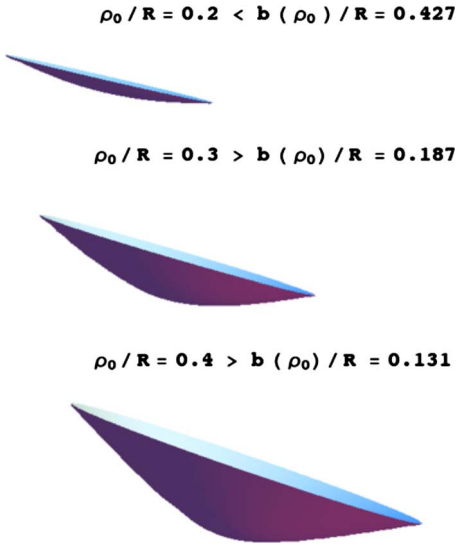

FIG. 3. (Color online) Minimum energy shapes of incomplete shells with a central pentamer as a function of the shell size, as determined by minimization of the stretching and bending energies. The buckling radius R_b was equal to $0.025R$. The dependence of $b(\rho_0)$ on the shell radius ρ_0 is nearly the same as the dotted line in Fig. 2 for $R_b/R \sim 0.03$ so the buckling transition is predicted to be in the range $b(\rho_0)/R \sim 0.13$ as is indeed the case.

If the dimensionless curvature radius R/R_b is reduced then, according to Fig. 2, the buckling threshold ρ_b drops below $\sqrt{384}R_b$ while the sharp drops of $b(\rho_0)$ and $\sigma_{\theta\theta}(\rho_0)$ are increasingly broadened. For R/R_b less than about 10, $b(\rho_0) \approx \sqrt{1/3}R$ and the buckling transition is nearly completely smeared out.

III. BOUNDARY OF THERMODYNAMIC STABILITY

After these preliminaries, we now can carry out the thermodynamic stability analysis. Specifically, we want to verify whether rotationally symmetric cap shapes represent, for a given shell area, the stable minimum free energy shape. This stability test is carried out by introducing an infinitesimal periodic modulation of the perimeter shape:

$$\rho(\theta) = \langle\rho\rangle + a_n \cos n\theta, \tag{13}$$

with n as an integer and with $a_n/\rho_0 \ll 1$. The total area A must remain the same as that of the spherical or conical cap, but the perimeter length P is allowed to increase. It is easy to show that, to first order in a_n/ρ_0, the mean radius has to be the disk radius of the symmetric cap so, to that order, $\langle\rho\rangle = \rho_0$. The binding energy of a subunit added to the perimeter of the shell is given by

$$\varepsilon(\theta) = \varepsilon_0 + \Omega\{\tau C(\theta) + U_e(\theta)\}. \tag{14}$$

Here, $\varepsilon_0 = -\Pi\Omega$ is the binding free energy of a subunit in the assembled shell far from the interface in the absence of elastic stress with Ω the surface area per capsomer and Π the cohesion free energy per unit area. The first term inside the brackets in Eq. (14) is the excess *Gibbs-Thompson* chemical potential of a particle placed on a curved surface separating

two thermodynamic phases in contact. Physically, it describes the work against the capillary pressure when a particle is added to a boundary. Next,

$$C(\theta) \approx (1/\rho_0)[1 + (n^2 - 1)(a_n/\rho_0)\cos n\theta] \tag{15}$$

is the local curvature of the perimeter line to first order in a_n/ρ_0. Finally, in the second term inside the brackets in Eq. (14), $U_e(\theta)$ is the elastic energy cost per unit area $(1/2)\sigma_{\alpha\beta}\mu_{\alpha\beta}$ evaluated at the perimeter. This term describes the price in elastic energy that must be paid when a subunit is added to the shell.

The chemical potential $\mu(\theta)$ of a subunit located along the perimeter is equal to $\varepsilon(\theta)$ plus a term that depends on the solution concentrations of subunits and shells but not on the stress or geometry of the perimeter. Within Gibbs theory, the thermodynamic stability of an interface is determined by the difference in chemical potentials of particles located at *protrusions* and at *indentations*. If this difference is positive, then a flux of particles from protrusions to indentations will anneal out any surface roughness, so a smooth interface is stable. If this difference is negative, then a flux of particles from indentations to protrusions will cause surface roughness to grow with time so a smooth interface is unstable. For example, the term $\tau C(\theta)$ in Eq. (14), which corresponds to a local capillary pressure, is higher than average for protrusions and lower than average for indentations, so it always has a stabilizing effect.

As before, the stress tensor at the interface must be obtained from an Airy function that must be a regular solution of the inhomogeneous biharmonic equation [Eq. (5)]. For the modulated boundary, this solution has the general form

$$\chi(r,\theta) = \chi(r) + a_n(\alpha_n r^{n+2} + \gamma_n r^n)\cos n\theta, \tag{16}$$

with $\chi(r)$ as the Airy stress function of the unperturbed shell. The parameters α_n and γ_n must be determined by the two boundary conditions $\sigma_{ij}n_j = -\tau C(\theta)n_i$ evaluated at the modulated border. To first order in a_n/ρ_0, the normal to the perimeter is here

$$\hat{n} \approx \hat{\rho} + \hat{\theta}\left(\frac{a_n}{\rho_0}\right)n \sin n\theta \tag{17}$$

to first order in a_n/ρ_0. After obtaining α_n and γ_n from the boundary conditions, the Airy function of the modulated state can, to first order in a_n/ρ_0, be expressed in terms of the tangential stress along the perimeter of the unperturbed shell shape as

$$\chi(r,\theta) = \chi(r) - \frac{1}{2}a_n\frac{\sigma^0_{\theta\theta}(\rho_0)}{\rho_0}(r/\rho_0)^n(r^2 - \rho_0^2)\cos n\theta - a_n\frac{\tau}{2\rho_0^2}(r/\rho_0)^n[(n-1)r^2 - (n+1)\rho_0^2]\cos n\theta. \tag{18}$$

The second term describes the modulation of the stretching or dilation elastic energy and the third term the modulation of the capillary stress.

The modulation of the chemical potential along the perimeter can now be evaluated using Eqs. (13)–(15) and (18). For $\tau/\rho_0 \gg \sigma^0_{\theta\theta}(\rho_0)$ the capillary contribution dominates and the modulated chemical potential reduces to

$$\mu(\theta) \approx \tilde{\mu}_0 + \Omega(n^2 - 1)\left(\frac{\tau}{\rho_0}\right)\left\{1 + 2\frac{(1-\nu)}{Y}\left(\frac{\tau}{\rho_0}\right)\right\} \times (a_n/\rho_0)\cos n\theta, \tag{19}$$

with $\tilde{\mu}_0 \sim \mu_0 + \Omega(\tau/\rho_0) + (\Omega/Y)(1-\nu)(\tau/\rho_0)^2$ and μ_0 as a constant independent of ρ_0. Both terms inside the curly brackets of Eq. (19) are due to capillary stress. The first term is the change in the Gibbs-Thompson contribution to the chemical potential due to the modulation while the second term is due to the elastic stresses that are generated by the variation of the capillary pressure $P_{cap}(\theta) = (\tau/\rho_0)[1 + (a_n/\rho_0)(n^2-1)\cos n\theta]$ along the perimeter of the shell. At protrusions $(\cos n\theta = 1)$ the chemical potential is always larger than the average value $\tilde{\mu}_0$, while at indentations $(\cos n\theta = -1)$, the chemical potential is always less than its average value. The circular perimeter is thus stable for $\tau/\rho_0 \gg \sigma^0_{\theta\theta}(\rho_0)$.

In the opposite regime $\tau/\rho_0 \ll \sigma^0_{\theta\theta}(\rho_0)$ where the noncapillary stress dominates, the modulated chemical potential along the perimeter is

$$\mu(\theta) \approx \tilde{\mu}_0 + \Omega\left\{\frac{\tau}{\rho_0}(n^2-1) - \frac{1}{Y}\left\{(2n+1)[\sigma^0_{\theta\theta}(\rho_0)]^2 - \frac{\rho_0}{2}\frac{d}{dr}[\sigma^0_{\theta\theta}(\rho_0)]^2\right\}\right\}(a_n/\rho_0)\cos n\theta, \tag{20}$$

with $\tilde{\mu}_0 \sim \mu_0 + \tau\Omega/\rho_0 + \frac{\Omega}{2Y}[\sigma^0_{\theta\theta}(\rho_0)]^2$. A circularly symmetric perimeter is stable if the expression in curly brackets is positive. The capillary contribution—the first term inside the curly brackets—is again stabilizing but the second term inside the curly brackets can have either sign. A sufficient condition for this term to be destabilizing would be for the perimeter stress $\sigma^0_{\theta\theta}(\rho_0)$ to decrease with increasing shell size although this is not a necessary condition for instability, as we will see. The stability condition can be expressed in the form of a critical value for the line energy:

$$\tau_n \approx \frac{\rho_0}{(n^2-1)Y}\left\{(2n+1)[\sigma^0_{\theta\theta}(\rho_0)]^2 - \frac{\rho_0}{2}\frac{d}{dr}[\sigma^0_{\theta\theta}(\rho_0)]^2\right\}. \tag{21}$$

Incomplete shells with circular perimeter are stable against a modulation with mode index n if the line energy exceeds τ_n.

A. Incomplete shell without central pentamer

We now are in a position to compare the thermodynamic stability of the two types of incomplete shells under consideration, using the perimeter tangential stress computed in the Appendix. For symmetric hexameric spherical caps, the tangential stress along the perimeter of the unperturbed shell generated by the spontaneous curvature increases proportional to the shell area as $\sigma^0_{\theta\theta} \approx -(Y/8)(\rho_0^2/R^2)$. The condition $\tau/\rho_0 \gg \sigma^0_{\theta\theta}(\rho_0)$ for dominance of the capillary stress thus reduces to $\tau \gg Y\rho_0^3/R^2$. Small spherical caps with $\tau \gg Y\rho_0^3/R^2$ are thus stable since capillary stresses have a stabilizing ef-

FIG. 4. (Color online) The $n=2$ mode. The dominant instability encountered in a thermodynamic stability analysis. The elongation of the shell allows relaxation of the perimeter stress.

fect. In the opposite limit, where $\tau \ll Y\rho_0^3/R^2$, the chemical potential of the modulated interface is, according to Eq. (20),

$$\mu(\theta) \approx \tilde{\mu}_0 + \Omega\left\{(n^2-1)\frac{\tau}{\rho_0} - (n-1)\frac{Y}{32}\left(\frac{\rho_0^4}{R^4}\right)\right\} \times (a_n/\rho_0)\cos n\theta \quad (\tau \ll Y\rho_0^3/R^2). \tag{22}$$

The critical line energy in terms of stability is thus $\tau_n(\rho_0) \approx (Y\rho_0/32(n+1))(\rho_0^4/R^4)$. The mode that goes unstable first with decreasing line energy is $n=2$, which corresponds to an ellipsoidal deformation of the shell shape (see Fig. 4). The shell becomes progressively less stable as the shell size increases further.

B. Incomplete shell with central pentamer

We show in the Appendix that if a single pentamer is located at the center of the incomplete shell, then for shell sizes below the buckling threshold the stress can be approximated as $\sigma^0_{\theta\theta}(r) \sim (Y/12)(\ln r/\rho_0 + 1)$. The condition $\tau/\rho_0 \ll \sigma^0_{\theta\theta}(\rho_0)$ for dominance of elastic stress now reduces to the requirement that $\tau \ll Y\rho_0$. By applying Eq. (21), the stability limit for the line energy is found to be

$$\tau_n(\rho_0) \approx \frac{Y\rho_0}{72(n^2-1)}\left\{n - \frac{1}{2}(2n-1)[\rho_0/b(\rho_0)]^2\right\}, \quad \rho_0 < (\sqrt{384})R_b. \tag{23}$$

We included in Eq. (23) the lowest-order correction term generated by the curvature stress. As the shell radius grows, the minimum line energy required for stability initially grows linearly with the radius. This increase begins to slow due to the correction term, as the shell size approaches the buckling threshold. By comparing Eqs. (22) and (23), it follows that below the buckling threshold a circularly symmetric patch of shell with a central pentamer is significantly *less stable* with respect to the AGTI, by a factor (R^4/ρ_0^4), than a shell of the same size without a central pentamer. On the other hand, beyond the buckling threshold the stability limit is

$$\tau_n(\rho_0) \approx \frac{576}{\pi^4}\frac{YR_b^4}{(n^2-1)\rho_0^3}\left[2(n+1)\ln^2\left(\frac{\pi\rho_0}{12R_b}\right) - \ln\left(\frac{\pi\rho_0}{12R_b}\right)\right], \quad \rho_0 > (\sqrt{384})R_b. \tag{24}$$

Now, the critical line energy *drops* with increasing shells size: a shell with a central pentamer that has passed the buckling transition becomes progressively more stable with respect to the AGTI. The buckling transition is thus a critical region in terms of thermodynamic stability. Assembling shells with a circular perimeter would be stable against the AGTI for *any* shell radius if there is no AGTI around the buckling transition. This condition is satisfied if the line energy exceeds the stability limit $\tau_{\max}$ for $n=2$ modes at the buckling threshold. Figure 5 shows that if $R/R_b \gg 1$ then the linear dependence of $\tau_2(\rho_0)$ on ρ_0 in Eq. (23) extends practically to the buckling threshold $\rho_0=\rho_b$. It follows from this observation that $\tau_{\max} \propto YR_b$. Numerically, we obtain $\tau_{\max} \approx 0.14YR_b$ for $R/R_b \gg 1$. Figure 5 shows that for smaller values of R/R_b, $\tau_{\max}$ is reduced compared to this value.

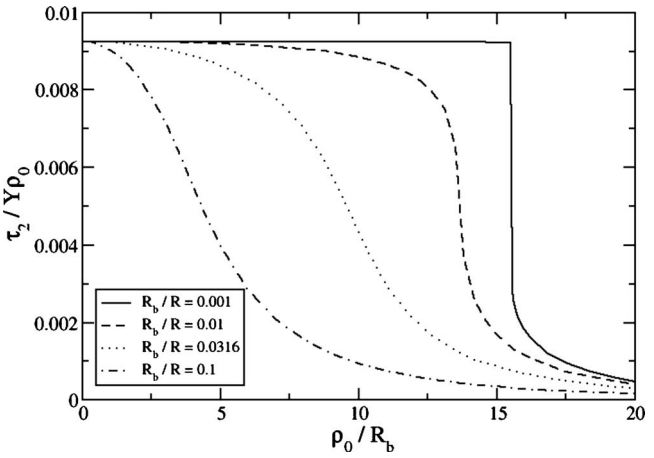

FIG. 5. The minimum line energy τ required for thermodynamic stability of a shell with central pentamer as a function of the shell radius for different values of the buckling radius, with $n=2$. Note that the vertical axis plots the ratio of τ and ρ_0. The maximum value for the minimum line energy is near the buckling transition, where the plot shows a sharp drop.

IV. GROWTH KINETICS

The determination of the stability limit of incomplete shells with circular perimeters was carried out within the bounds of equilibrium thermodynamics. It is known from the studies of the AGTI in the context of epitaxial growth that the most rapidly growing unstable mode cannot be determined by thermodynamic considerations alone. In this section we will investigate a simple kinetic model for the instability in order to identify the most rapidly growing unstable mode, which will lead to other useful results as well.

For epitaxial growth, AGTI kinetics is dominated by the transport of particles in response to the chemical potential gradients along the interface. This can take place either by diffusion through the vapor or solution ("evaporation or recondensation") in contact with the solid or by diffusion along the interface [14]. Both mechanisms in principle would be possible for viral shells as well, but in view of the high reported off-rates, we will restrict ourselves to the evaporation or recondensation mechanism. Consider a partial viral shell in contact with a solution that contains a certain low concentration $c(\infty)$ of subunits. In the limit of low concentrations, the *on-rate* k^+ for subunits in solution (or an oligomer of subunits) to be added to the perimeter of the shell is

diffusion limited. According to the Smoluchowski theory of diffusion-limited reactions, the on-rate k^+ is then given by $4\pi aDc(\infty)$. Here, D is the subunit diffusion coefficient and a is the "reaction radius" for subunit capture by the shell perimeter. If one assumes, as we will, that the reaction radius for capture of a subunit is determined solely by the structure of individual subunits (or oligomers), then the on-rate is independent of the geometry of the partial shell. According to the principle of detailed balance, the *off-rate* k^- for a perimeter subunit to be released back into solution is then given by $k^-=k^+c_0 \exp \beta\varepsilon$, with (minus) ε as the subunit or oligomer binding energy along the perimeter and with c_0 as a constant with the units of concentration. The off-rate thus depends on both the local shape of the perimeter and on the local elastic stress along the perimeter through the binding energy $\varepsilon(\theta)=\varepsilon_0+\Omega\{\tau C(\theta)+U_e(\theta)\}$ of Eq. (14).

The time-dependent shape of the perimeter will be expanded in a Fourier series $\rho(\theta,t)=\rho_0(t)+\Sigma_n a_n(t)\cos n\theta$. We showed earlier that if the capillary pressure τ/ρ_0 is large compared to the perimeter elastic stress $\sigma^0_{\theta\theta}(\rho_0)$, then the shell is stable. We will focus below on the opposite case where τ/ρ_0 is less than $\sigma^0_{\theta\theta}(\rho_0)$ and use Eq. (20). Using $k^-(\theta)/k^+=c_0 \exp[\beta\varepsilon(\theta)]$, one can expand $\exp[\beta\varepsilon(\theta)]$ to lowest order in powers of (a_n/ρ_0):

$$k^-(\theta)/\langle k^-\rangle_{\rho_0} \approx \left(1+\beta\Omega\sum_{n>1}\left\{\frac{\tau}{\rho_0}(n^2-1)-\frac{1}{Y}\left\{(2n+1)\times[\sigma^0_{\theta\theta}(\rho_0)]^2-\frac{\rho_0}{2}\frac{d}{dr}[\sigma^0_{\theta\theta}(\rho_0)]^2\right\}\right\}\times(a_n/\rho_0)\cos n\theta\right). \quad (25)$$

The *angular-averaged* off-rate $\langle k^-\rangle_{\rho_0}$ is here given by

$$\langle k^-\rangle_{\rho_0} \sim k^+c_0 \exp\beta\left\{\varepsilon_0+\tau\Omega/\rho_0+\frac{\Omega}{2Y}[\sigma^0_{\theta\theta}(\rho_0)]^2\right\}. \quad (26)$$

Equating the radial growth velocity $\frac{\partial\rho(\theta,t)}{\partial t}=\frac{d\rho_0}{dt}+\Sigma_n\frac{da_n}{dt}\cos n\theta$ with the growth velocity $v_n=a[k^+c(\infty)-k^-(\theta)]$ along the normal to the perimeter leads to separate equations for the amplitude of each mode:

$$\frac{d\rho_0}{dt} \propto a(k^+c(\infty)-\langle k^-\rangle_{\rho_0}), \quad (27)$$

$$\frac{da_n}{dt} \approx -a\langle k^-\rangle_{\rho_0}\beta\Omega\left\{\frac{\tau}{\rho_0}(n^2-1)-\frac{1}{Y}\left\{(2n+1)[\sigma^0_{\theta\theta}(\rho_0)]^2-\frac{\rho_0}{2}\frac{d}{dr}[\sigma^0_{\theta\theta}(\rho_0)]^2\right\}\right\}a_n/\rho_0. \quad (28)$$

Using Eqs. (27) and (28), we can again investigate the two different shell geometries.

A. Incomplete shell without central pentamer

If we use in Eq. (26) the perimeter stress appropriate for a spherical cap composed purely of hexamers, then the angular-average off-rate reduces to

$$\langle k^-\rangle_{\rho_0} \sim k^+c_0 \exp\beta\left(\varepsilon_0+\tau\Omega/\rho_0+\frac{1}{128}\Omega Y(\rho_0^4/R^4)\right). \quad (29)$$

Initially, for small shell sizes, the off-rate decreases with increasing shell radius, when capillary effects still dominate. Then, for shell radii larger than $\rho^*=(32\tau R^4/Y)^{1/5}$, the off-rate starts to increase with shell radius, as the stretching stress generated by the shell curvature takes over. Let $\langle k^-\rangle_{\rho^*}$ be the minimum off-rate separating these two regimes. For low concentrations, with $k^+c(\infty)$ less than $\langle k^-\rangle_{\rho^*}$, shells are unable to even start forming, due to this curvature-induced elastic stress. If the concentration is increased and $k^+c(\infty)$ exceeds $\langle k^-\rangle_{\rho^*}$, then shell growth becomes possible. It is easy to show that this condition is obeyed if the subunit concentration exceeds the threshold $c(\infty)^*/c_{eq}=\exp[(5/4)\beta\Omega(\tau/\rho^*)]$, where $c_{eq}/c_0=\exp\beta\varepsilon_0$ is the bulk concentration at which subunits in solution are in chemical equilibrium with stress-free shells. If the concentration exceeds $c(\infty)^*$, then the average growth rate $d\rho_0/dt \propto a(k^+c(\infty)-\langle k^-\rangle_{\rho_0})$ has two *zeros* as a function of the shell radius denoted by ρ_- and ρ_+. These zeros act as fixed points for the growth equation. Close to $c(\infty)^*$, their location is given by

$$(\rho_\pm-\rho^*)/\rho^* \approx \pm\left\{\frac{\rho^*}{(5/2)\beta\tau\Omega}\ln[c(\infty)/c(\infty)^*]\right\}^{1/2}. \quad (30)$$

The first zero, ρ_-, is an *unstable* fixed point. If the initial radius is less than this unstable fixed point, then the shell shrinks. The shell grows if the initial radius exceeds the unstable fixed point. The unstable fixed point thus has the same properties as the usual critical nucleus of the classical theory of nucleation and growth. The second zero is a *stable* fixed point. At ρ_+, the increasing elastic energy cost of the growing shell starts to exceed the free energy gain. As a result the *average* radius of the shell stops growing. A hexameric shell without pentamers will naturally evolve to this fixed point. However, the shape of the shell at this fixed point need *not* be rotationally symmetric. Assume that the average radius of the shell equals ρ_+. In Eq. (28), each mode then has a time-independent growth rate ω_n, with $da_n/dt=\omega_n a_n$, given by

$$\omega_n \approx a\langle k^-\rangle_{\rho_+}\rho_+^{-1}\beta\Omega(n-1)\left\{-\frac{\tau}{\rho_+}(n+1)+\frac{Y}{32}\left(\frac{\rho_+^4}{R^4}\right)\right\}. \quad (31)$$

At the onset concentration $c(\infty)^*$ for shell growth, where ρ_+ equals $\rho^*=(32\tau R^4/Y)^{1/5}$, ω_n is negative for positive n but with increasing free subunit concentrations, ω_n becomes positive for larger and larger n, in which case the circular shell is unstable [the critical concentration for the nth mode to become unstable is found by using Eq. (30) in Eq. (31) and setting the term in curly brackets to zero]. At the stable fixed point, the shell is thus in general not circular. The most rapidly growing mode is *not* $n=2$ but instead the mode with

index closest to $n^*=(Y/64\tau)(\rho_+^5/R^4)$. Note that though we obtained this result from kinetic arguments, it does not depend on the kinetic parameters. The full determination of the actual shell shape at the fixed point is however beyond linear stability analysis.

B. Incomplete shell with central pentamer

For a hexameric shell with a central pentamer and curvature radius R large compared to the buckling radius, the off-rate is given by

$$\langle k^- \rangle_{\rho_0} \sim \begin{cases} k^+ c_0 \exp \beta \left\{ \varepsilon_0 + \tau\Omega/\rho_0 + \frac{1}{288}\Omega Y \left[1 - \frac{3}{2}\left(\frac{\rho_0}{R}\right)^2 \right]^2 \right\}, & \rho_0 \ll \sqrt{384} R_b \\ k^+ c_0 \exp \beta \left[\varepsilon_0 + \tau\Omega/\rho_0 + \frac{288}{\pi^4}\Omega Y \left(\frac{R_b}{\rho_0}\right)^4 \ln^2\left(\frac{\pi\rho_0}{12R_b}\right) \right], & \rho_0 \gg \sqrt{384} R_b. \end{cases} \tag{32}$$

The off-rate now always *decreases* with shell size. At the buckling transition the drop is particularly sharp. For very large shell sizes, the off-rate approaches the equilibrium value $k^+c_0 \exp \beta\varepsilon_0$. Because the off-rate decreases monotonically with shell size over the whole range, the rate $k^+c(\infty)-\langle k^- \rangle_{\rho_0}$ can have only one zero. This zero is an unstable fixed point and corresponds to the critical nucleus of conventional nucleation and growth theory. The buckling transition prevents here the stress build-up that "suffocates" the growth of pentamer-free shells.

We saw earlier that if the line energy exceeds the threshold $\tau_{\max}$, then AGTI-free growth is possible. If this condition is not obeyed, then unstable modes will be most pronounced near the buckling threshold. At the buckling threshold itself, the growth rate is estimated as

$$\omega_n \approx a\langle k^- \rangle_{\rho_0} (\beta\Omega/\sqrt{384}R_b) \left\{ -\frac{\tau}{\sqrt{384}R_b}(n^2-1) + 2n\frac{Y}{144} \right\} \tag{33}$$

using $\sigma^0_{\theta\theta}(r) \sim (Y/12)(\ln r/\rho_0 + 1)$. The most rapidly growing mode at the buckling transition has a mode index closest to $n^* \sim 0.14YR_b/\tau$, again independent of kinetic parameters. If we view n^*/R_b as a *wavelength* for the AGTI at the buckling transition, then we recover the classical result that the wavelength of the most unstable mode is determined by the ratio of the elastic modulus and the interface energy. Finally, it is easy to show that when the radius exceeds a threshold $\rho_n \propto [(1/(n-1))(Y/\tau)R_b^4]^{1/3}$, the amplitude of the nth mode will start to decrease with time.

V. CONCLUSION

We found that assembling shells of large viruses should be subject to the AGTI unless the buckling instability intervenes. Many large viral shells, such as the $T=13$ shell of herpes simplex, are characterized by a very high degree of structural order and reproducibility. Since for conventional solids the AGTI leads to loss of structural order, our results suggest that for large viruses the AGTI must be avoided, presumably by buckling. Is this possible? In order to examine this question, one must estimate the threshold $\tau_{\max} \approx 0.14YR_b$ for stable growth and compare this with estimates for the line energy itself. Interestingly, the estimate of $\tau_{\max}$ for viral shells in fact can be directly obtained from studies of the *mechanical deformability* of shells. First, rewrite YR_b as $\sqrt{Y\kappa}$. Next, we recall that the "spring constant" for indenting a thin shell is given by $2.5\sqrt{Y\kappa/R}$ according to continuum theory [15]. This spring constant has been measured by atomic-force microscopy for different viral shells under different conditions [16] and the quantity $\sqrt{Y\kappa}$ was found to vary over a limited range. For a shell with a 12 nm inner radius (cowpea chlorotic mottle virus), this spring constant is, for example, about 0.2 N/m [17]. That means that $\sqrt{Y\kappa} \sim 0.9 \times 10^{-9}$ N for that shell. The corresponding stability limit of the line energy would be about $\tau_{\max} \approx 0.12$ nN. The line energy τ itself has never been measured but the "natural" value for the line energy τ would be the ratio of the characteristic energy scale for capsid subunit interactions, which is about $10k_BT$, and the characteristic length scale, which is the size of a subunit (about one nanometer). This leads to a line energy τ of about 10 pN. This is about an order of magnitude less than $\tau_{\max} \approx 0.12$ nN, which suggests that an AGTI still should be expected. Actually, the proposition that τ could be even as large as 10 pN is quite questionable. The thermodynamic energy barrier of the "critical nucleus" for capsid assembly is a hemisphere with a perimeter $2\pi R$. The "transition state" free energy thus equals $2\pi R\tau$ in the absence of elastic stress and the presence of elastic stress can only increase the height of this activation barrier. For a large shell like herpes simplex, with a radius R in the range of 50 nm, $2\pi R\tau$ would be hundreds of k_BT for τ in the pN range. From kinetic studies of viral assembly [18], there is no experimental evidence for huge thermodynamic activation energy barriers of this size. The line energy is thus actually expected to be quite small on the pN scale.

This indicates that the AGTI cannot be avoided during viral assembly even if buckling takes place. This need not be a paradox. Viral shells are not *exactly* like two-dimensional crystals: 12 pentamers must be inserted at appropriate sites in order to produce an icosahedron. During an AGTI, the chemical potential of subunits located inside indentations is higher than that of protrusions due to the excess perimeter

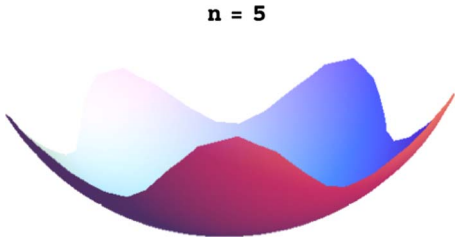

FIG. 6. (Color online) The $n=5$ mode. If $n=5$ would be the most rapidly growing AGTI unstable mode at the buckling transition then this could set the stage for proper insertion of additional pentamers.

stress. This "stress-condensation" actually might be a precursor for the insertion of fivefold disclinations, i.e., pentamers. In this view, an AGTI instability might be a *necessary* step for the proper assembly of a shell. An $n=5$ mode (see Fig. 6) would be, for example, favorable for shell assembly for pentamer-seeded growth. This would lead to an interesting scenario where the combination of the buckling instability and AGTI guides the insertion of subsequent pentamers. This would however require a careful "fine tuning" of $n^* \sim 0.14YR_b/\tau$ to be close to five. Interestingly, a recent numerical simulation of a hexameric growing shell indeed encountered an AGTI followed by stress-condensation, which heralded the appearance of disclinations along the growth perimeter [19].

We should conclude by noting that all our results were obtained using continuum elasticity theory. For smaller capsids, with low T numbers, continuum theory is not expected to apply due to discrete structure of the shell. It is known, from the study of the growth of solid materials, that lattice anisotropy introduced by molecular-level discreteness weakens growth instabilities [20]. Numerical studies we are currently carrying out indicate that assembly of small T icosahedral shells is indeed not affected by the growth instability discussed in this paper.

ACKNOWLEDGMENTS

We would like to thank Joe Rudnick and Bill Klug for helpful discussions. This work was supported by the NSF under DMR Grant No. 04-04507.

APPENDIX

We need to solve

$$\Delta^2\chi(\vec{r}) + Y[K(\vec{r}) - s(\vec{r})] = 0 \tag{A1}$$

with disclination density $s(\vec{r}) = (2\pi/6)\delta(\vec{r})$ and Gaussian curvature $K(\vec{r}) = \zeta_{xx}\zeta_{yy} - \zeta_{xy}^2$ for the trial function $\zeta(r) = \sqrt{s/\pi}(r^2 + b^2)^{1/2}$ subject to the boundary condition $\sigma_{ij}n_j = -(\tau/\rho_0)n_i$ along a circular perimeter of radius ρ_0. For this trial function, the Gaussian curvature

$$K(r) = \frac{b^2 s}{\pi(r^2 + b^2)^2} \tag{A2}$$

has a maximum at the origin and then decays as $1/r^4$ for large r. Equation (A1) is linear and can be solved by standard methods. We need only consider radially symmetric solutions. By substitution it can be checked that Eq. (A1) is solved by

$$\chi(r) = \frac{Ys}{16\pi}\left\{2r^2 \ln\left(\frac{r}{\rho_0}\right) + r^2 \ln\left(\frac{\rho_0^2 + b^2}{r^2 + b^2}\right) + b^2\left(\frac{r^2}{\rho_0^2}\right) \times \ln\left[1 + \left(\frac{\rho_0^2}{b^2}\right)\right] - b^2 \ln\left[1 + \left(\frac{r^2}{b^2}\right)\right] + b^2 Li_2\left(-\frac{r^2}{b^2}\right)\right\} - \frac{\tau}{2\rho_0}r^2 \tag{A3}$$

that satisfies the boundary conditions. Here, $Li_2(x) = -\int_0^x (\ln(1-t))/t\,dt$ is the dilogarithm function. For the linear stability analysis [Eq. (21)], the noncapillary contribution $\sigma^0_{\theta\theta}(r) = d^2\chi(r)/dr^2 + \tau/\rho_0$ to tangential component of the stress tensor and its derivative are needed. From Eq. (A3) we find

$$\sigma^0_{\theta\theta}(r) = \frac{Ys}{8\pi}\left\{2\ln\left(\frac{r}{\rho_0}\right) + \ln\left(\frac{\rho_0^2 + b^2}{r^2 + b^2}\right) + \left(\frac{b^2}{\rho_0^2}\right)\ln\left[1 + \left(\frac{\rho_0^2}{b^2}\right)\right] + \left(\frac{b^2}{r^2}\right)\ln\left[1 + \left(\frac{r^2}{b^2}\right)\right]\right\}. \tag{A4}$$

The tangential component of the stress tensor and its derivative in Eq. (21) were computed from Eq. (A4). Using Eq. (6), the complete noncapillary contribution to stretching energy is

$$F_s = -\frac{Ys^2b^2}{32\pi}\left\{(1 + b^2/\rho_0^2)\left[\ln\left(1 + \frac{\rho_0^2}{b^2}\right)\right]^2 + 2Li_2\left(-\frac{\rho_0^2}{b^2}\right)\right\}, \tag{A5}$$

while the bending energy $F_b = \kappa/2\int d^2s(H - 2/R)^2$ with $H = \Delta\zeta$ equals

$$F_b = \kappa\left\{\frac{1}{2}s\ln(1 + \rho_0^2/b^2) + 2\pi\rho_0^2/R^2 - 4\sqrt{\pi s}\frac{\rho_0^2}{R\sqrt{\rho_0^2 + b^2}} - \frac{b^4 s}{4(\rho_0^2 + b^2)^2} - \frac{b^2 s}{(\rho_0^2 + b^2)} + \frac{5}{4}s\right\} \tag{A6}$$

for $\zeta(r) = \sqrt{s/\pi}(r^2 + b^2)^{1/2}$. Minimizing the sum of stretching and bending energies with respect to $x = \rho_0/b$ leads to the final result:

$$4\sqrt{\pi s}(\rho_0/R)\frac{x}{(1 + x^2)^{3/2}} + s\left(\frac{1}{(1 + x^2)^3} + \frac{1}{(1 + x^2)^2} - \frac{1}{1 + x^2} - 1\right) - \frac{1}{16\pi}\left(\frac{s\rho_0}{xR_b}\right)^2 \times \left\{\left(1 + \frac{2}{x^2}\right)[\ln(1 + x^2)]^2 + 2Li_2(-x^2)\right\} = 0, \tag{A7}$$

with $R_b = \sqrt{\kappa/Y}$ as the buckling radius. In the limit of small x, the solution of Eq. (A7) reduces to Eq. (11).

For small x, we can expand the left hand side of Eq. (A7) in powers of x. Using $Li_2(x) \approx x + (1/4)x^2 + (1/9)x^3 + \cdots$ gives

$$4\sqrt{\pi s}(\rho_0/R) + \left(\frac{s^2\rho_0^2}{32\pi R_b^2} - 4s\right)x - 6\sqrt{\pi s}(\rho_0/R)x^2 + 8sx^3 + \cdots = 0. \quad \text{(A8)}$$

If both x and ρ_0/R are small compared to one, it is consistent to retain only the first two terms, which leads to Eq. (11) of the text. For large x, $Li_2(x\to-\infty)\approx-(1/2)(\ln x)^2-\pi^2/6$ and Eq. (A7) simply reduces to $-s+\pi s^2\rho_0^2/48R_b^2x^2\approx 0$ for ρ_0/R small compared to one.

[1] For a review: T. S. Baker, N. H. Olson, and S. D. Fuller, Microbiol. Mol. Biol. Rev. **63**, 862 (1999).

[2] D. L. D. Caspar and A. Klug, Cold Spring Harbor Symp. Quant. Biol. **27**, 1 (1962).

[3] H. Fraenkel-Conrat and R. C. Williams, Proc. Natl. Acad. Sci. U.S.A. **41**, 690 (1955); P. J. Butler and A. Klug, Sci. Am. **239**(5), 62 (1978); A. Klug, Philos. Trans. R. Soc. London, Ser. B **354**, 531 (1999).

[4] W. K. Kegel and P. van der Schoot, Biophys. J. **91**, 1501 (2006).

[5] J. M. Johnson, J. Tang, Y. Nyame, D. Willits, M. J. Young, and A. Zlotnick, Nano Lett. **5**, 765 (2005).

[6] P. Ceres and A. Zlotnick, Biochemistry **41**, 11525 (2002).

[7] J. Lidmar, L. Mirny, and D. R. Nelson, Phys. Rev. E **68**, 051910 (2003).

[8] See, for example, *Thin Film Materials: Stress, Defect, and Formation and Surface*, edited by L. B. Freund and S. Suresh (Cambridge University Press, Cambridge, 2009).

[9] F. Yang, Mech. Mater. **38**, 111 (2006).

[10] H. S. Seung and D. R. Nelson, Phys. Rev. A **38**, 1005 (1988).

[11] R. Zandi, P. van der Schoot, D. Reguera, W. Kegel, and H. Reiss, Biophys. J. **90**, 1939 (2006).

[12] M. A. Krol, N. H. Olson, J. Tate, J. E. Johnson, T. S. Baker, and P. Ahlquist, Proc. Natl. Acad. Sci. U.S.A. **96**, 13650 (1999); RNA-controlled polymorphism in the in vivo assembly of 180-subunit and 120-subunit virions from a single capsid protein. Institute for Molecular Virology, University of Wisconsin, Madison, WI 53706, USA.

[13] J. Tang, J. M. Johnson, K. A. Dryden, M. J. Young, A. Zlotnick, and J. E. Johnson, J. Struct. Biol. **154**, 59 (2006).

[14] D. J. Srolovitz, Acta Metall. **37**, 621 (1989).

[15] L. D. Landau and E. M. Lifshitz, *Theory of Elasticity* (Pergamon, New York, 1986).

[16] I. L. Ivanovska, P. J. de Pablo, B. Ibarra, G. Sgalari, F. C. MacKintosh, J. L. Carrascosa, C. F. Schmidt, and G. J. Wuite, Proc. Natl. Acad. Sci. U.S.A. **101**, 7600 (2004); J. P. Michel, I. L. Ivanovska, M. M. Gibbons, W. S. Klug, C. M. Knobler, G. J. L. Wuite, and C. F. Schmidt, *ibid.* **103**, 6184 (2006).

[17] W. S. Klug, R. F. Bruinsma, J. P. Michel, C. M. Knobler, I. L. Ivanovska, C. F. Schmidt, and G. J. Wuite, Phys. Rev. Lett. **97**, 228101 (2006).

[18] G. L. Casini, D. Graham, D. Heine, R. L. Garcea, and D. T. Wu, Virology **325**, 320 (2004).

[19] W. Klug (private communication).

[20] See, for example, E. Rolley, S. Balibar, and F. Gallet, Europhys. Lett. **2**, 247 (1986).